THE JOURNAL OF BIOLOGICAL CHEMISTRY VOL. 287, NO. 20, pp. 16541–16549, May 11, 2012


# Human Cyclin-dependent Kinase 2-associated Protein 1 (CDK2AP1) Is Dimeric in Its Disulfide-reduced State, with Natively Disordered N-terminal Region*[S]

Received for publication, February 7, 2012, and in revised form, March 10, 2012 Published, JBC Papers in Press, March 15, 2012, DOI 10.1074/jbc.M112.343863

**Asli Ertekin[‡§1], James M. Aramini[‡], Paolo Rossi[‡], Paul G. Leonard[‡¶‖], Haleema Janjua[‡], Rong Xiao[‡], Melissa Maglaqui[‡], Hsiau-Wei Lee[**], James H. Prestegard[**], and Gaetano T. Montelione[‡¶2]**

*From the [‡]Center for Advanced Biotechnology and Medicine and Northeast Structural Genomics Consortium and the [§]BioMaPS Institute for Quantitative Biology, Rutgers, The State University of New Jersey, Piscataway, New Jersey 08854, the [¶]Department of Biochemistry, Robert Wood Johnson Medical School-University of Medicine & Dentistry of New Jersey, Piscataway, New Jersey 08854, and the [‖]Howard Hughes Medical Institute and the **Complex Carbohydrate Research Center and Northeast Structural Genomics Consortium, University of Georgia, Athens, Georgia 30602*

**Background:** CDK2AP1 is a tumor suppressor important in cancer biology.
**Results:** CDK2AP1 forms a four-helix dimeric structure. The disordered N-terminal region contains an IκB kinase ϵ phosphorylation site.
**Conclusion:** The CDK2AP1 dimer does not require a disulfide bond, but the structure is poised for disulfide bond formation.
**Significance:** The three-dimensional structure supports a potential role for disulfide bond formation in functional regulation of CDK2AP1.

**CDK2AP1 (cyclin-dependent kinase 2-associated protein 1), corresponding to the gene *doc-1* (deleted in oral cancer 1), is a tumor suppressor protein. The *doc-1* gene is absent or down-regulated in hamster oral cancer cells and in many other cancer cell types. The ubiquitously expressed CDK2AP1 protein is the only known specific inhibitor of CDK2, making it an important component of cell cycle regulation during $G_1$-to-S phase transition. Here, we report the solution structure of CDK2AP1 by combined methods of solution state NMR and amide hydrogen/deuterium exchange measurements with mass spectrometry. The homodimeric structure of CDK2AP1 includes an intrinsically disordered 60-residue N-terminal region and a four-helix bundle dimeric structure with reduced Cys-105 in the C-terminal region. The Cys-105 residues are, however, poised for disulfide bond formation. CDK2AP1 is phosphorylated at a conserved Ser-46 site in the N-terminal "intrinsically disordered" region by IκB kinase ϵ.**

CDK2AP1 (cyclin-dependent kinase 2-associated protein 1; $p12^{DOC-1}$) is a highly conserved tumor suppressor protein corresponding to the gene *doc-1* (deleted in oral cancer 1) (supplemental Fig. S1). It was first identified by subtractive hybridization experiments using hamster oral cancer cells, where it was observed that the gene product is absent or reduced in malignant cells. When transformed keratinocytes are transfected with *doc-1*, its expression inhibits cell growth (1). A ubiquitously expressed, highly conserved homolog of this gene with 88% cDNA identity and 98% protein sequence identity has also been identified in different human tissues (2, 3). In three malignant human oral keratinocyte cell lines analyzed, the expression of the *doc-1* gene was absent or reduced beyond detection (3), similar to previous results on hamster models (2). These early findings suggested an important role for CDK2AP1 protein in carcinogenesis.

In recent years, the importance of CDK2AP1 in various cancer cell lines has been intensively investigated. Differential expression of CDK2AP1 was observed for two phenotypes of human colorectal cancer cells, microsatellite stable and unstable cell lines (4). In another study of 180 gastric cancer tissues, negative expression of CDK2AP1 was reported for 78% of the tissues, which was directly correlated with more advanced tumor stages and invasion (5). *doc-1* gene therapy in mouse models of head and neck squamous cell carcinoma results in significant reduction in the weight, size, and growth of tumors compared with control systems, suggesting the utility of CDK2AP1 as a therapeutic target (6). Ectopic expression of *doc-1* in transfected malignant hamster keratinocyte models was observed to elevate the number of apoptotic cells, implying a possible role for CDK2AP1 in apoptotic pathways (7). In addition to its role in carcinogenesis, it was observed that *doc-1* is one of the 216 genes enriched in stem cells, making it an important marker defining the "stemness" of the cell (8). Furthermore, CDK2AP1 is associated with embryonic development, and low levels of this protein lead to embryonic lethality (9).

* This work was supported, in whole or in part, by National Institutes of Health Protein Structure Initiative Grant U54-GM-094597 from NIGMS.
[S] This article contains supplemental "Materials and Methods," Figs. S1–S15, and additional references.
*The atomic coordinates and structure factors (code 2kw6) have been deposited in the Protein Data Bank, Research Collaboratory for Structural Bioinformatics, Rutgers University, New Brunswick, NJ (http://www.rcsb.org/).*
*Complete $^{1}H$, $^{13}C$, and $^{15}N$ resonance assignments for CDK2AP1(61–115) have been deposited in the Biological Magnetic Resonance Data Bank (http://www.bmrb.wisc.edu) under BMRB accession number 16808.*
[1] Supported by a Jerome and Lorraine Aresty Cancer Biology Fellowship and a National Institutes of Health Interdisciplinary Research Workforce Fellowship 5 R90 DK071502.
[2] To whom correspondence should be addressed: CABM, Rutgers University, 679 Hoes Lane, Piscataway, NJ 08854. Tel.: 732-235-5321; Fax: 732-235-5779; E-mail: guy@cabm.rutgers.edu.

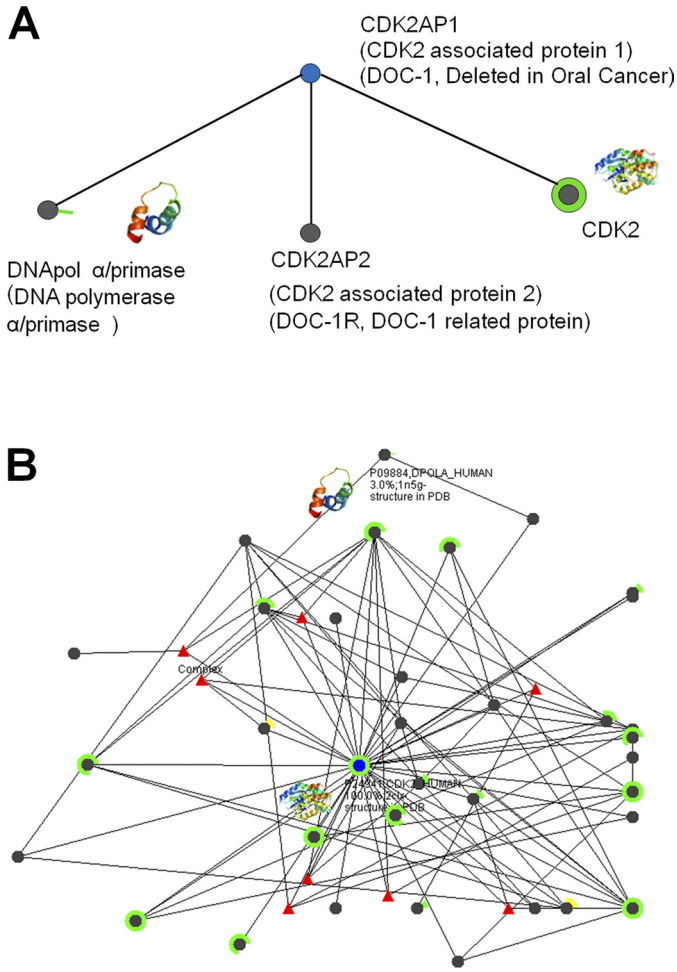


FIGURE 1. **Interactomes for CDK2AP1 (*A*) and CDK2 (*B*).** Each *black node* represents a protein that interacts with the query protein (*blue node*). *Edges* indicate that there are literature data for the corresponding protein-protein interactions. The *partial* or *complete rings* around some nodes indicate the fraction of the corresponding protein sequence for which a three-dimensional structure is available in the Protein Data Bank (*green rings*) or that can be homology-modeled from a structure in the Protein Data Bank with >80% sequence identity (*yellow rings*). Some of the three-dimensional structures of interaction partners are shown as *miniature ribbon diagrams*. These graphical analyses were adopted from the Human Cancer Protein Interaction Network website (62).

Published Western blot and immunoblot experiments on cell lysates using GST-tagged CDK2AP1 have revealed three putative binding partners (Fig. 1): (i) DNA polymerase α/primase (DNA pol α/primase)[3] (10), (ii) DOC-1R (deleted in oral cancer 1-related; CDK2AP2) (11), and (iii) CDK2 (12). DNA pol α/primase and CDK2 are important in cell cycle regulation. *In vitro* analyses have shown that the first six amino acid residues of CDK2AP1 interact with DNA pol α/primase, the only protein that can initiate *de novo* DNA replication (13). It was observed that the CDK2AP1-DNA pol α/primase interaction negatively regulates DNA replication at the level of initiation, suggesting a novel mechanism for S phase regulation (3, 10). However, there have been no subsequent reports in the literature to support these data or that shed light on the details of this interaction.

[3] The abbreviations used are: pol α, polymerase α; HDX-MS, hydrogen/deuterium exchange mass spectrometry; IKKε, IκB kinase ε; RDC, residual dipolar coupling.

DOC-1R/CDK2AP2, another reported binding partner of CDK2AP1 (11), is a close homolog of CDK2AP1, with 57% overall sequence identity. DOC-1R/CDK2AP2 is a substrate of MAPK and appears to be important in microtubule organization during meiotic maturation (14). However, there have not been any further studies elucidating the function of this protein in the cell or the details of its interactions with CDK2AP1.

CDK2AP1 has also been observed to interact specifically with free non-phosphorylated CDK2, making it the only known specific inhibitor of CDK2 (12). CDK2 regulates the $G_1$-to-S phase transition of the cell cycle through its complexes with cyclins A and E (15). It was observed that CDK2AP1 inhibits CDK2 kinase activity by sequestering the inactive monomer, preventing formation of complexes with cyclins A and E and/or by directing it to the proteasome degradation pathway (12). Thus, DNA replication is inhibited by CDK2AP1 through inhibition of CDK2 and/or inhibition of DNA pol α/primase. This scenario is consistent with the previous observation that transfected malignant keratinocytes experience significantly reduced cell growth and reversion of phenotype (1). Overexpression of CDK2AP1 consistently results in alteration of the cell cycle profile, with increased $G_1$ phase and reduced S phase (12).

More recently, stable isotope labeling studies with the Mi-2/NuRD (nucleosome remodeling and histone deacetylase) chromatin-remodeling complex revealed that CDK2AP1 is also a subunit of the Mi-2/NuRD complex (16) and may be involved in epigenetic gene regulation. However, the molecular function of CDK2AP1 within this complex is still unknown.

Although the importance of CDK2AP1 in cell cycle regulation and tumor formation has been clearly established, no structural data have been reported to date. Here, we report the three-dimensional solution NMR structure of CDK2AP1 (UniProtKB/Swiss-Prot ID CDKA1_HUMAN and Northeast Structural Genomics Consortium ID HR3057). The N-terminal 60 residues of full-length dimeric CDK2AP1 are "intrinsically disordered" based on hydrogen/deuterium exchange mass spectrometry (HDX-MS) analysis (17). The solution structure of the C-terminal region of CDK2AP1 (CDK2AP1(61–115)), determined under conditions in which Cys-105 is in a reduced form, is a homodimeric four-helix bundle.

Kim *et al.* (18) have suggested that interchain disulfide bond formation between Cys-105 residues is essential for CDK2AP1 function. As intracellular disulfide bond formation is unusual, their conclusion is very interesting. Our NMR studies demonstrate that the dimeric structure of CDK2AP1 does not require disulfide bond formation. However, the locations of the two Cys-105 residues in the structure reveal that they are indeed poised for interchain disulfide bond formation. Our studies also demonstrate that CDK2AP1 contains a phosphorylation site for IκB kinase ε (IKKε) (19) at Ser-46, which is located in the intrinsically disordered N-terminal region of the protein structure.

## EXPERIMENTAL PROCEDURES

*Preparation of Protein Samples*—Samples of full-length CDK2AP1, truncated version CDK2AP1(61–115), and mutant CDK2AP1(61–115)-C105A were cloned, expressed, and puri-

fied following the standard protocols of the Northeast Structural Genomics Consortium (20); a complete description of the methods used in this work is presented under supplemental "Materials and Methods." HDX-MS experiments on full-length CDK2AP1 were carried out following the procedure outlined by Sharma *et al.* (17). Samples of uniformly $^{13}C$,$^{15}N$- and 5% $^{13}C$,U-$^{15}N$-enriched human CDK2AP1(61–115) and CDK2AP1(61–115)-C105A for NMR structure determination were concentrated to 0.7–0.9 mM in 95% $H_2O$ and 5% $^2H_2O$ solution containing 20 mM MES, 200 mM NaCl, 10 mM DTT, and 5 mM $CaCl_2$ (pH 6.5). Analytical gel filtration with static light scattering data demonstrated that both full-length and truncated CDK2AP1 are dimeric in solution under the conditions used in the NMR studies.

*Analytical Ultracentrifugation Analysis of CDK2AP1-(61–115)*—Sedimentation velocity experiments were performed at 25 °C using a ProteomeLab Optima XL-I analytical ultracentrifuge (Beckman Coulter) with interference optics. 400-μl samples were loaded into double-sector Epon centerpieces and centrifuged at 50,000 rpm. Data analysis was performed using SEDPHAT Version 8.2 (21). The partial specific volume of CDK2AP1(61–115) was estimated to be 0.7290 ml/g from its amino acid sequence using SEDNTERP Version 1.09. The solvent density and viscosity were estimated using SEDNTERP Version 1.09 (22).

*Solution Structure Calculation Protocols*—All NMR data were collected at 25 °C on Varian INOVA 600-MHz and Bruker AVANCE 800-MHz NMR spectrometers equipped with 5-mm cryoprobes. Complete $^1H$, $^{13}C$, and $^{15}N$ resonance assignments for CDK2AP1(61–115) were determined using conventional triple-resonance NMR methods (23) and deposited in the Biological Magnetic Resonance Data Bank (BMRB accession number 16808). Resonance assignments were validated using the AVS (assignment validation suite) software package (24). The dimer interface in CDK2AP1(61–115) was identified using $^{13}C$-filtered NOESY experiments (25) on a 1:1 sample of $^{13}C$,$^{15}N$-enriched and unlabeled (natural abundance) protein. Residual dipolar coupling (RDC) data were collected for two bond vectors, N-$H^N$ and N-C′, in a single alignment medium (see supplemental "Materials and Methods" for details). The CDK2AP1(61–115) structure was calculated using CYANA Version 3.0 (26–28), and the 20 models out of 100 with the lowest target function were refined by restrained molecular dynamics in explicit water using CNS Version 1.1 (29); all structure calculations were performed with the intra- and interchain NOE data and RDC data included. The final refined ensemble of 20 models has been deposited in the Protein Data Bank (code 2kw6). Structural statistics and global structure quality factors, including Verify3D (30), ProsaII (31), *PROCHECK* (32), and MolProbity (33) raw and statistical *Z*-scores, were computed using the PSVS Version 1.3 software package (34). Values for the global goodness of fit of the final structure ensembles with the NOESY peak list data were determined using the RPF analysis program (35).

*Phosphorylation by IKKε*—IKKε was purchased from Invitrogen (catalog number PV4875). The reaction solution was prepared with 0.1 mM full-length CDK2AP1 in 50 mM Tris (pH 7.5), 200 mM NaCl, 10 mM $CaCl_2$, 5 mM β-glycerol phosphate, and 2.5 mM ATP. The phosphorylation reaction was initiated by injecting 4 μl of 4 μM IKKε and incubated at 17 °C for 48 h. The extent of phosphorylation was confirmed by LC-MS/MS experiments.

## RESULTS

*HDX-MS Analysis*—Residues comprising unstructured or intrinsically disordered regions in a protein can be readily identified by HDX-MS (17) because the exchange rates of these amide hydrogens are significantly higher than those in structured regions due to their solvent accessibilities (36). Assessment of amide exchange rates and solvent accessibility by HDX-MS provides a reliable method of identifying structurally disordered polypeptide segments of proteins (17, 37). Moreover, construct optimization involving the elimination of unstructured elements identified by HDX-MS can significantly improve success rates of both crystallization experiments for x-ray crystallography studies and protein structure determination by solution NMR methods (17, 37, 38).

Full-length CDK2AP1 was analyzed by HDX-MS. The backbone amide groups in the entire N-terminal 60 residues of the protein exhibit rapid HDX rates characteristic of intrinsically disordered polypeptide segments (Fig. 2). Based on this information, a truncated construct corresponding to residues 61–115 was designed for NMR structural studies. The resonance frequencies of highly dispersed peaks in $^1H$-$^{15}N$ heteronuclear single-quantum correlation spectra for full-length and truncated CDK2AP1 are very similar (supplemental Fig. S2), demonstrating that removal of the disordered N-terminal region does not disrupt the overall structure in the ordered C-terminal region of the protein.

*CDK2AP1(61–115) Is a Dimer in Solution*—Western blot analyses of contact-inhibited human diploid cells using anti-CDK2AP1 polyclonal antibody and SDS-PAGE demonstrated that CDK2AP1 can occur in the cell in both disulfide-reduced (interpreted as monomeric) and disulfide-bonded (interpreted as dimeric) forms (18). Interestingly, in the contact inhibition phase, the disulfide-bonded "dimeric" form of CDK2AP1 increases with a concomitant decrease in the disulfide-reduced "monomeric" form. Mutational analysis further confirmed that when the cysteine residue at position 105 is replaced with an alanine residue, preventing formation of the disulfide-bonded dimer, the inhibition of CDK2 by CDK2AP1 is suppressed. This study concluded that the Cys-105 disulfide-bonded dimer is the active form of CDK2AP1 (18).

We analyzed the oligomerization state of CDK2AP1(61–115) using analytical gel filtration with static light scattering, sedimentation velocity analytical ultracentrifugation, and $^{15}N$ NMR relaxation measurements. All of these techniques firmly established that CDK2AP1(61–115) is a dimer in solution, with $K_d < 10$ μM, under the conditions used in this study (Fig. 3 and supplemental Figs. S3–S5). Analytical gel filtration with static light scattering experiments further demonstrated that the full-length CDK2AP1 protein is also predominantly dimeric in solution (supplemental Fig. S5), *i.e.* both the full-length and C-terminal domains of CDK2AP1 form stable dimers under reducing conditions.

*Solution Structure of CDK2AP1(61–115)*—The solution NMR structure of dimeric CDK2AP1(61–115) was determined

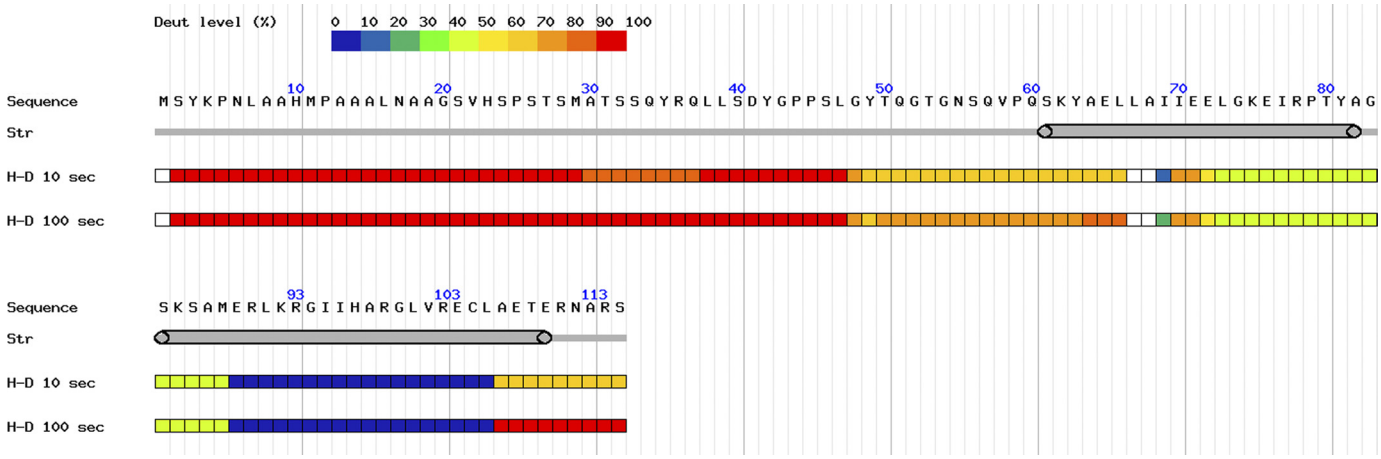


FIGURE 2. **HDX-MS results for CDK2AP1.** Back-exchange corrected deuteration (*Deut*) levels were estimated on a per residue basis and were derived from 36 overlapping peptide fragments and are shown according to the color coding indicated. Peptide fragments from the *red* regions exhibit essentially 100% amide proton exchange in the indicated time frame, whereas peptide fragments in the *blue* regions exhibit essentially no amide proton exchange in the corresponding time frame. Amide proton $^{1}H/^{2}H$ exchange times (*H-D*) were 10 and 100 s. Secondary structural elements are shown below the protein sequence information.

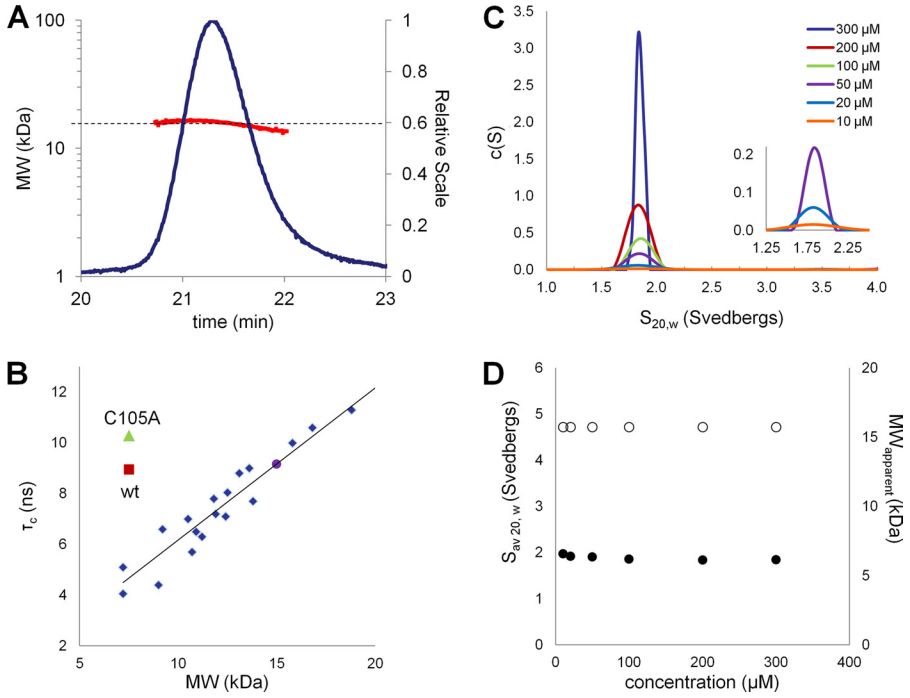


FIGURE 3. *A*, static light scattering results for CDK2AP1(61–115). 30 μl of 6 mg/ml CDK2AP1(61–115) in 20 mM MES (pH 6.5), 200 mM NaCl, 5 mM $CaCl_2$, 10 mM DTT, 1× protease inhibitors, and 0.02% $NaN_3$ was injected onto an analytical gel filtration column (PROTEIN KW-802.5, Shodex, Kawasaki, Japan), with the effluent monitored by refractive index (*blue trace*; Optilab rEX) and 90° static light scattering (miniDAWN TREOS, Wyatt Technology) detectors. The resulting experimental molecular mass of CDK2AP1(61–115) is 15.98 kDa (*red*); the expected molecular mass for the single chain including an affinity tag is 7.42 kDa, demonstrating that it forms a dimeric structure. *B*, rotational correlation time ($\tau_c$) *versus* molecular mass plotted for known monomeric proteins (*blue*), CDK2AP1(61–115) (*red*), and CDK2AP1(61–115)-C105A (*green*) constructs. CDK2AP1 samples were in 20 mM MES (pH 6.5) containing 0.02% $NaN_3$, 10 mM DTT, 5 mM $CaCl_2$, 200 mM NaCl, 1× protease inhibitors, 10% $^{2}H_2O$, and 50 μM sodium 4,4-dimethyl-4-silapentane-1-sulfonic acid (DSS) at 25 °C. *C* and *D*, sedimentation velocity analysis of CDK2AP1(61–115) dissolved in 20 mM HEPES, 200 mM NaCl, 5 mM $CaCl_2$, and 10 mM DTT (pH 7.0). *C*, the *c*(*s*) distribution plots for CDK2AP1(61–115) protein samples at 10–300 μM (as indicated in the *inset*) and centrifuged at 50,000 rpm. *D*, the weight average sedimentation coefficient for CDK2AP1(61–115) (●) and the apparent molar mass of the protein (○) have been plotted *versus* the loaded protein concentration.

using triple-resonance NMR, RDC data, and X-filtered NOESY experiments. Structural statistics are summarized in Table 1. The structure was determined using 1827 NOE-based distance restraints, including 230 interchain restraints derived from X-filtered NOESY and iterative NOESY assignment, 72 RDC data, and 182 dihedral restraints obtained based on the backbone chemical shift data. These provided some 18.3 restraints per residue, including 2.1 interchain restraints per residue. The average backbone root mean square deviation of ordered residues in the final ensemble is 0.6 Å. Backbone dihedral angle analysis indicated that 99.3% of the residues fall in the most favored regions of the Ramachandran plot (33). Overall, the structure quality scores, including RPF scores (35), comparing the structure with the unassigned NOESY peak lists (summarized in Table 1) indicate a high quality solution NMR structure for the dimeric C-terminal domain of CDK2AP1.

**TABLE 1**

**Summary of NMR and structural statistics for human CDK2AP1(61–115)**

Structural statistics were computed for the ensemble of 20 NMR structures deposited in the Protein Data Bank. r.m.s., root mean square; r.m.s.d., root mean square deviation.

| | |
|---|---|
| **Completeness of resonance assignments**[a] | |
| Backbone (%) | 97.4 |
| Side chain (%) | 84.4 |
| Aromatic (%) | 100 |
| Stereospecific methyl (%) | 100 |
| **Conformationally restricting constraints**[b] | |
| Distance constraints | |
| Total | 1827 |
| Intraresidue ($i = j$) | 560 |
| Sequential ($\|i - j\| = 1$) | 433 |
| Medium range ($1 < \|i - j\| \leq 5$) | 434 |
| Long range ($\|i - j\| > 5$) | 400 |
| Intrachain | 170 |
| Interchain | 230 |
| Distance constraints per residue | 16.6 |
| Dihedral angle constraints | 182 |
| No. of constraints per residue | 18.3 |
| No. of long-range constraints per residue | 3.6 |
| No. of interchain constraints per residue | 2.1 |
| **Residual constraint violations**[b] | |
| Average no. of distance violations per structure | |
| 0.1–0.2 Å | 4.05 |
| 0.2–0.5 Å | 0.40 |
| >0.5 Å | 0 |
| Average r.m.s. distance violation/constraint (Å) | 0.01 |
| Maximum distance violation (Å) | 0.30 |
| Average no. of dihedral angle violations per structure | |
| 1–10° | 1.85 |
| >10° | 0 |
| Average r.m.s. dihedral angle violation/constraint (°) | 0.22 |
| Maximum dihedral angle violation (°) | 4.80 |
| **r.m.s.d. from average coordinates (all/ordered)**[b,c] | |
| Backbone atoms (Å) | 2.8/0.6 |
| Heavy atoms (Å) | 3.3/1.2 |
| **Ramachandran statistics for ordered residues (Richardson MolProbity)**[b,c] | |
| Most favored regions (%) | 99.3 |
| Additionally allowed regions (%) | 0.7 |
| Disallowed regions (%) | 0.0 |
| **Global quality scores (raw/*Z*-score)**[b] | |
| Verify3D | 0.41/−0.80 |
| ProsaII | 1.07/1.74 |
| *PROCHECK* ($\phi$-$\psi$)[c] | 0.54/2.44 |
| *PROCHECK* (all)[c] | 0.42/2.48 |
| MolProbity Clash | 13.76/−0.84 |
| **RPF scores**[d] | |
| Recall | 0.961 |
| Precision | 0.868 |
| *F*-measure | 0.913 |
| DP-score | 0.738 |
| **RDC statistics**[e] | |
| No. of $D_{NH}$ constraints | 36 |
| $R$ | 0.913 ± 0.011 |
| $Q_{r.m.s.}$ | 0.133 ± 0.009 |
| No. of $D_{NC}$ constraints | 36 |
| $R$ | 0.988 ± 0.001 |
| $Q_{r.m.s.}$ | 0.115 ± 0.006 |

[a] Values were computed using AVS software from the expected number of peaks, excluding highly exchangeable protons (N-terminal, and Lys amino groups, Arg guanido protons, and hydroxyls of Ser, Thr, and Tyr), carboxyls of Asp and Glu, non-protonated aromatic carbons, and the C-terminal tag.

[b] Values were calculated using PSVS Version 1.4. Average distance violations were calculated using the sum over $r^{-6}$.

[c] Ordered residue ranges ($S(\phi) + S(\psi) > 1.8$): residues 62–112.

[d] RPF scores reflect the goodness of fit of the final ensemble of structures (including disordered residues) to the NMR data.

[e] RDC statistics were computed by PALES (63).

Each protomer of CDK2AP1(61–115) is composed of two helices, including residues 61–82 ($\alpha$1) and 84–112 ($\alpha$2), connected by a type II $\beta$-turn to form a hairpin helix motif. These hairpin helices dimerize to form an antiparallel four-helix bundle (Fig. 4) that has 2-fold rotational symmetry about an axis nearly parallel to the helix axes and vertical in Fig. 4*A*. The orientation of this axis was confirmed by independently generating an alignment tensor from two sets of RDC data (39).

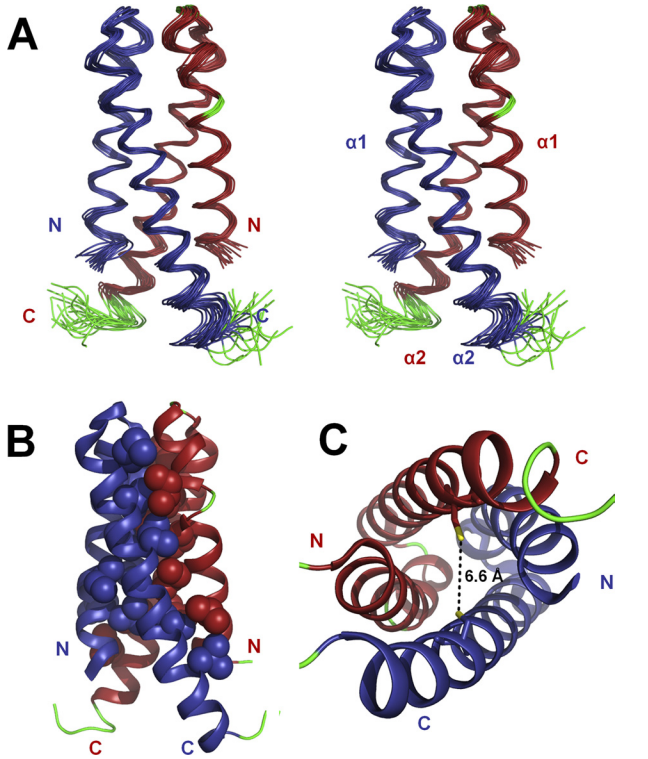


FIGURE 4. **Solution NMR structure of CDK2AP1(61–115).** *A*, ensemble of the 20 lowest energy NMR-derived conformers in stereoview. *B*, lowest energy conformer showing hydrophobic side chains that stabilize the interface in a space-filling representation. *C*, top-down view of the four-helix dimeric structure with the side chains of the Cys-105 residues shown in stick representation. The thiol groups of the two Cys-105 residues are nearby one another in the three-dimensional structure and poised for disulfide bonding. In *A–C*, $\alpha$-helices are shown in *blue* (chain 1) and *red* (chain 2), the loops and not well defined N- and C-terminal regions are shown in *green*, and the sulfur atoms of the Cys-105 residues are shown in *yellow*.

The four-helix bundle structure is predominantly stabilized by hydrophobic interactions involving numerous hydrophobic residues at the dimer interface (Fig. 4*B*). Although this fold is relatively rare, similar dimeric protein folds have been reported for a microtubule-binding protein (Protein Data Bank code 1wu9) and a phycobilisome degradation protein (Protein Data Bank code 1ojh), which are significantly different in sequence and do not appear to be homologs of CDK2AP1.

The $\alpha$1-helix exhibits a kink at Gly-74–Lys-75 near the $\beta$-turn, deviating from an ideal linear helical structure. This kink allows intrachain hydrophobic interactions of side chains of Ala-87 with Thr-80 and of Pro-79 and Thr-80 with Leu-91 and interchain interactions of Ile-77 with Ile-95. The electrostatic potential map indicates that the surface of the interchain $\alpha$1-$\alpha$2 interface has a net positive charge near the loop region and, to a lesser extent, a net negative charge near N- and C-terminal regions of the chains (supplemental Fig. S6).

Based on SDS-PAGE analysis, it has been proposed that interchain disulfide bond formation between Cys-105 residues is essential for the "dimerization" of CDK2AP1 (18). Under the reducing conditions used in our sample preparation, which

included 10 mM DTT, the Cys-105 thiol groups are in reduced states. This was confirmed by the C$\beta$ chemical shift value of Cys-105 (26.20 ppm), which is diagnostic of the reduced oxidation state of the associated thiol group (40, 41). Disulfide mapping using MALDI-TOF analysis further confirmed that 10 mM DTT is sufficient to fully reduce the Cys residues of CDK2AP1(61–115) to cysteine (supplemental Fig. S7). Sedimentation velocity experiments, carried out under these reducing conditions using protein concentrations ranging from 10 to 300 $\mu$M and summarized in Fig. 3 (*C* and *D*), demonstrated that the CDK2AP1 dimer, with reduced cysteine residues, is relatively stable, with $K_d < 10$ $\mu$M. Hence, our structure and biophysical data do not support previously published results concerning the requirement for disulfide bonding of Cys-105 residues in dimer formation (18).

*Mutation C105A Does Not Disrupt CDK2AP1(61–115) Dimerization*—To verify that dimer formation by CDK2AP1 does not require disulfide bond formation, the single-site C105A mutant of CDK2AP1(61–115) was also studied by NMR. Kim *et al.* (18) have reported that the C105A mutation abolishes both dimer formation and *in vivo* CDK2-inhibiting activity of CDK2AP1. $^{15}$N relaxation measurements, providing an estimate of the rotational correlation time ($\tau_c$), demonstrated that CDK2AP1(61–115)-C105A is dimeric under the same conditions used to determine the solution NMR structure of wild-type CDK2AP1(61–115) (Fig. 3*B* and supplemental Fig. S3). Furthermore, comparison of the $^{1}$H-$^{15}$N heteronuclear single-quantum correlation spectra of WT CDK2AP1(61–115) and mutant CDK2AP1(61–115)-C105A (supplemental Fig. S8) confirmed that the two structures are essentially identical, with minor chemical shift perturbations located mostly in the vicinity of the mutation site. It is not surprising that the C105A mutant retains a dimeric structure because the dimer interface of WT CDK2AP1 is stabilized by an extensive network of hydrophobic interactions (Fig. 4*B*).

The thiol groups of the two reduced Cys residues are in relatively close proximity in the structure of the WT protein, *i.e.* 6.6 $\pm$ 0.8 Å distance between sulfur atoms (Fig. 4*C*). Restrained energy minimization calculations carried out with disulfide bond restraints between Cys-105 sulfur atoms demonstrated that the four-helix dimeric structure requires only minor adjustments to accommodate a disulfide bond. Hence, the structure of disulfide-reduced CDK2AP1(61–115) is poised for Cys-105 disulfide bond formation. However, our extensive biophysical data on CDK2AP1(61–115)-C105A clearly demonstrate that disulfide bonding of Cys-105 is not required for dimer formation.

*CDK2AP1 Is Phosphorylated by IKK*$\epsilon$—The IKK complex is part of the canonical cellular mechanism that regulates propagation of cellular responses to inflammation through inactivation of inhibitors of NF-$\kappa$B and the resulting activation of NF-$\kappa$B pathways (42). A less studied IKK family protein, IKK$\epsilon$ is a Ser/Thr kinase and has been shown to regulate the interferon response mechanism, as well the canonical NF-$\kappa$B pathways (43, 44). IKK$\epsilon$ has also been identified as an oncogene and is overexpressed in 30% of breast cancer cell lines (45–47). Several targets of IKK$\epsilon$ kinase have been identified in interferon signaling pathways, but it is not yet clear which targets are most important for cell transformation (19).

Recently, a consensus phosphorylation peptide motif for IKK$\epsilon$, *XXX*(Y/F/P/M)*X*pS(L/I/F)*X*(Y/W/F)*X*, was identified by peptide library scanning studies (19). A proteome-based bioinformatics search for this motif revealed a set of possible phosphorylation targets for IKK$\epsilon$. In a search against the Swiss-Prot sequence data base (48), the Ser-46 site in CDK2AP1 scored in the top 0.05% of sites searched, predicting CDK2AP1 as a candidate IKK$\epsilon$ target (19).

To validate this prediction and the role of phosphorylation in the structure of CDK2AP1, we carried out *in vitro* phosphorylation studies on full-length CDK2AP1 using GST-tagged IKK$\epsilon$ (Invitrogen PV4875). Based on LC-MS/MS analysis, complete phosphorylation was observed at Ser-46 (supplemental Figs. S9 and S10). NMR experiments demonstrated that there are no significant structural changes in the full-length protein due to this phosphorylation (supplemental Fig. S11). In cases in which the structures of other candidate IKK$\epsilon$ targets are known, the predicted phosphorylation sites are located in both structured and unstructured regions. For CDK2AP1, the Ser-46 phosphorylation site is located in the disordered region of the protein, as determined by HDX-MS analysis.

## DISCUSSION

In this study, we have presented spectroscopic, structural, and mutagenesis studies on CDK2AP1. Our studies indicate that the N-terminal ~60 residues of CDK2AP1 are intrinsically disordered. The C-terminal structured region forms a homodimeric four-helix bundle, stabilized by an extensive hydrophobic interface.

We have also shown that IKK$\epsilon$ phosphorylates CDK2AP1 *in vitro* at Ser-46, which is located in the disordered N-terminal region of the protein. This is the first demonstration that CDK2AP1 is a substrate for IKK$\epsilon$. In a recent large-scale study of phosphorylation dynamics during the cell cycle, it was reported that Ser-24 of CDK2AP1 is phosphorylated during mitosis (49). However, in this proteomics study, it was not clear which kinase was responsible for the observed phosphorylation. Although Ser-24, like Ser-46, is located in the disordered N-terminal region of CDK2AP1, in our *in vitro* study, there was no evidence for phosphorylation of Ser-24 by IKK$\epsilon$.

Intrinsically disordered proteins and protein segments are used in nature with increasing occurrence from bacteria to eukaryotes (50). Fully and partially disordered eukaryotic proteins are often involved in cellular processes like transcriptional regulation, signaling, cell cycle control, differentiation, and other aspects of cancer biology (51). The lack of a rigid native structure enables post-translational modification sites to be readily available and structural flexibility for higher order promiscuity in protein-protein interactions, and it can provide stability in complex formation especially in entropy-driven complexes (50, 52–56). Because of this structural plasticity, these proteins are frequently observed as hubs or binding partners to hub proteins in protein-protein interaction networks (57).

Intrinsic disorder has been observed in other CDK inhibitor proteins. For example, p21$^{Cip1}$ and p27$^{Kip1}$ are intrinsically dis-

ordered and fold into secondary structures only when bound to CDK-cyclin complexes (58–60). This structural flexibility allows them to bind to different CDK-cyclin complexes, providing functional diversity (61).

We do not yet know if similar structural changes take place during CDK2AP1 interaction with CDK2. The long unstructured region of CDK2AP1 may function to provide solvent accessibility of the phosphorylation sites Ser-24 and Ser-46 or structural plasticity to bind to multiple proteins, including DNA pol α/primase, DOC-1R, CDK2, and the Mi-2/NuRD complex. The functional importance of the intrinsically disordered N-terminal region of CDK2AP1 remains to be elucidated in further studies.

Our analysis has demonstrated that CDK2AP1 is a stable dimer in solution, even in the absence of interchain disulfide bond formation. No dimer dissociation was observed under reducing conditions and concentrations as low as 10 μM. Comparison of the $^{15}N$ and $^{13}C$ heteronuclear single-quantum correlation spectra of full-length and truncated constructs demonstrated that removing the disordered N-terminal segment did not disrupt the structure of the four-helix dimer. This conclusion is also supported by the observation that the full-length protein is also a dimer in solution under reducing conditions. However, the concentration of the protein in cellular conditions is not known. At much lower concentrations, CDK2AP1 may dissociate into a monomeric state.

The dimeric structure of CDK2AP1 determined in this work by NMR provides valuable insights into structure-function relationships. The activation of CDK2AP1 as an inhibitor of CDK2 in contact-inhibited human diploid cells has been attributed to "dimer formation," resulting from interchain disulfide bond formation, which is detected under denaturing conditions by SDS-PAGE (18). Moreover, it was reported that the extent of disulfide-stabilized "dimer formation" is regulated at different stages of the cell cycle. Replacing Cys-105 with alanine abolished both dimer formation and the CDK2-inhibiting function of the protein. However, this SDS-PAGE analysis was carried out under denaturing conditions, which would disrupt any noncovalent dimers that may be present. Although these data provide evidence correlating disulfide bond formation between CDK2AP1 molecules with contact inhibition, they do not provide information on the oligomeric state of the protein in the cell. In particular, our work has demonstrated that dimer formation may occur even in the absence of disulfide bond formation.

The thiol groups of the Cys-105 residues are sufficiently close in the dimer interface of the three-dimensional structure to allow disulfide bond formation without significantly altering the structure. However, we cannot exclude the possibility that minor structural changes that may accompany such disulfide bond formation may modulate the protein's function.

Cys-105 disulfide bond formation in the cell can regulate the CDK2-inhibiting function of CDK2AP1 (18). These results were interpreted as arising from homodimerization of CDK2AP1. However, the homologous CDK2AP2 (DOC-1R) protein, in which Cys-105 is strictly conserved, also binds CDK2AP1 (11). Indeed, there is 85% sequence identity between CDK2AP1 and CDK2AP2 in the ordered C-terminal region of CDK2AP1 that forms the four-helix bundle (*i.e.* residues 61–115). This interaction could potentially form a disulfide-linked CDK2AP1-CDK2AP2 heterodimer, with a structure similar to the CDK2AP1 homodimer shown in Fig. 4. Such a heterodimer might not be distinguished from a CDK2AP1 homodimer in Western blot/SDS-PAGE analysis (18).

In light of the three-dimensional homodimeric structure of CDK2AP1 with reduced Cys-105 reported in this work, the results of Kim *et al.* (18) may be interpreted in two ways depending on the local concentrations of CDK2AP1 and CDK2AP2 in their functional environments in the cell. On the one hand, the functional concentrations of CDK2AP1 and CDK2AP2 in the cell may be very low, and disulfide bond formation may stabilize the small fraction of homo- or heterodimeric CDK2AP1 molecules, shifting the equilibrium in favor of a dimeric structure. Alternatively, a significant fraction of reduced homo- or heterodimeric CDK2AP1 may be present prior to its activation by disulfide bond formation within the dimeric structure. Further studies will be required to distinguish these distinct mechanisms of CDK2AP1 activation by disulfide bond formation and the potential role of heterodimerization with CDK2AP2. In either case, however, it is interesting that disulfide bond formation inside the cell, which is indeed supported by the juxtaposition of Cys-105 thiol groups in the native three-dimensional homodimeric structure of CDK2AP1, may modulate the CDK2-regulating function of CDK2AP1.

*Acknowledgments—We thank C. Ciccosanti, J. Everett, M. Jiang, P. Lobel, A. Lemak, B. Rost, G. V. Swapna, and H. Zheng for valuable scientific discussions.*

## REFERENCES

1. Todd, R., McBride, J., Tsuji, T., Donoff, R. B., Nagai, M., Chou, M. Y., Chiang, T., and Wong, D. T. (1995) Deleted in oral cancer-1 (*doc-1*), a novel oral tumor suppressor gene. *FASEB J.* **9,** 1362–1370
2. Daigo, Y., Suzuki, K., Maruyama, O., Miyoshi, Y., Yasuda, T., Kabuto, T., Imaoka, S., Fujiwara, T., Takahashi, E., Fujino, M. A., and Nakamura, Y. (1997) Isolation, mapping, and mutation analysis of a human cDNA homologous to the *doc-1* gene of the Chinese hamster, a candidate tumor suppressor for oral cancer. *Genes Chromosomes Cancer* **20,** 204–207
3. Tsuji, T., Duh, F. M., Latif, F., Popescu, N. C., Zimonjic, D. B., McBride, J., Matsuo, K., Ohyama, H., Todd, R., Nagata, E., Terakado, N., Sasaki, A., Matsumura, T., Lerman, M. I., and Wong, D. T. (1998) Cloning, mapping, expression, function, and mutation analyses of the human ortholog of the hamster putative tumor suppressor gene *doc-1*. *J. Biol. Chem.* **273,** 6704–6709
4. Yuan, Z., Sotsky Kent, T., and Weber, T. K. (2003) Differential expression of DOC-1 in microsatellite-unstable human colorectal cancer. *Oncogene* **22,** 6304–6310
5. Choi, M. G., Sohn, T. S., Park, S. B., Paik, Y. H., Noh, J. H., Kim, K. M., Park, C. K., and Kim, S. (2009) Decreased expression of p12 is associated with more advanced tumor invasion in human gastric cancer tissues. *Eur. Surg. Res.* **42,** 223–229
6. Figueiredo, M. L., Kim, Y., St. John, M. A., and Wong, D. T. (2005) $p12^{CDK2\text{-}AP1}$ gene therapy strategy inhibits tumor growth in an *in vivo* mouse model of head and neck cancer. *Clin. Cancer Res.* **11,** 3939–3948
7. Cwikla, S. J., Tsuji, T., McBride, J., Wong, D. T., and Todd, R. (2000) *doc-1*-mediated apoptosis in malignant hamster oral keratinocytes. *J. Oral Maxillofac. Surg.* **58,** 406–414
8. Ramalho-Santos, M., Yoon, S., Matsuzaki, Y., Mulligan, R. C., and Melton,

D. A. (2002) "Stemness": transcriptional profiling of embryonic and adult stem cells. *Science* **298,** 597–600
9. Kim, Y., McBride, J., Kimlin, L., Pae, E. K., Deshpande, A., and Wong, D. T. (2009) Targeted inactivation of $p12^{Cdk2ap1}$, CDK2-associating protein 1, leads to early embryonic lethality. *PLoS ONE* **4,** e4518
10. Matsuo, K., Shintani, S., Tsuji, T., Nagata, E., Lerman, M., McBride, J., Nakahara, Y., Ohyama, H., Todd, R., and Wong, D. T. (2000) $p12^{DOC\text{-}1}$, a growth suppressor, associates with DNA polymerase α/primase. *FASEB J.* **14,** 1318–1324
11. Buajeeb, W., Zhang, X., Ohyama, H., Han, D., Surarit, R., Kim, Y., and Wong, D. T. (2004) Interaction of the CDK2-associated protein-1, $p12^{DOC\text{-}1/CDK2AP1}$, with its homolog, $p14^{DOC\text{-}1R}$. *Biochem. Biophys. Res. Commun.* **315,** 998–1003
12. Shintani, S., Ohyama, H., Zhang, X., McBride, J., Matsuo, K., Tsuji, T., Hu, M. G., Hu, G., Kohno, Y., Lerman, M., Todd, R., and Wong, D. T. (2000) $p12^{DOC\text{-}1}$ is a novel cyclin-dependent kinase 2-associated protein. *Mol. Cell. Biol.* **20,** 6300–6307
13. Wang, T. S. (1996) *DNA Replication in Eukaryotic Cells*, Cold Spring Harbor Laboratory Press, Plainview, NY
14. Terret, M. E., Lefebvre, C., Djiane, A., Rassinier, P., Moreau, J., Maro, B., and Verlhac, M. H. (2003) DOC-1R: a MAP kinase substrate that controls microtubule organization of metaphase II mouse oocytes. *Development* **130,** 5169–5177
15. Satyanarayana, A., and Kaldis, P. (2009) Mammalian cell cycle regulation: several CDKs, numerous cyclins, and diverse compensatory mechanisms. *Oncogene* **28,** 2925–2939
16. Spruijt, C. G., Bartels, S. J., Brinkman, A. B., Tjeertes, J. V., Poser, I., Stunnenberg, H. G., and Vermeulen, M. (2010) CDK2AP1/DOC-1 is a *bona fide* subunit of the Mi-2/NuRD complex. *Mol. BioSyst.* **6,** 1700–1706
17. Sharma, S., Zheng, H., Huang, Y. J., Ertekin, A., Hamuro, Y., Rossi, P., Tejero, R., Acton, T. B., Xiao, R., Jiang, M., Zhao, L., Ma, L. C., Swapna, G. V., Aramini, J. M., and Montelione, G. T. (2009) Construct optimization for protein NMR structure analysis using amide hydrogen/deuterium exchange mass spectrometry. *Proteins* **76,** 882–894
18. Kim, Y., Ohyama, H., Patel, V., Figueiredo, M., and Wong, D. T. (2005) Mutation of Cys-105 inhibits dimerization of $p12^{CDK2\text{-}AP1}$ and its growth suppressor effect. *J. Biol. Chem.* **280,** 23273–23279
19. Hutti, J. E., Shen, R. R., Abbott, D. W., Zhou, A. Y., Sprott, K. M., Asara, J. M., Hahn, W. C., and Cantley, L. C. (2009) Phosphorylation of the tumor suppressor CYLD by the breast cancer oncogene IKKε promotes cell transformation. *Mol. Cell* **34,** 461–472
20. Acton, T. B., Xiao, R., Anderson, S., Aramini, J., Buchwald, W. A., Ciccosanti, C., Conover, K., Everett, J., Hamilton, K., Huang, Y. J., Janjua, H., Kornhaber, G., Lau, J., Lee, D. Y., Liu, G., Maglaqui, M., Ma, L., Mao, L., Patel, D., Rossi, P., Sahdev, S., Shastry, R., Swapna, G. V., Tang, Y., Tong, S., Wang, D., Wang, H., Zhao, L., and Montelione, G. T. (2011) Preparation of protein samples for NMR structure, function, and small-molecule screening studies. *Method Enzymol.* **493,** 21–60
21. Schuck, P. (2003) On the analysis of protein self-association by sedimentation velocity analytical ultracentrifugation. *Anal. Biochem.* **320,** 104–124
22. Laue, T. M., Shah, B. D., Ridgeway, T. M., and Pelletier, S. L. (1992) in *Analytical Ultracentrifugation in Biochemistry and Polymer Science* (Harding, S. E., Rowe, A. J., and Horton, J., eds) pp. 90–125, Royal Society of Chemistry, Cambridge, United Kingdom
23. Aramini, J. M., Huang, Y. J., Swapna, G. V., Cort, J. R., Rajan, P. K., Xiao, R., Shastry, R., Acton, T. B., Liu, J., Rost, B., Kennedy, M. A., and Montelione, G. T. (2007) Solution NMR structure of *Escherichia coli ytfP* expands the structural coverage of the UPF0131 protein domain family. *Proteins* **68,** 789–795
24. Moseley, H. N., Sahota, G., and Montelione, G. T. (2004) Assignment validation software suite for the evaluation and presentation of protein resonance assignment data. *J. Biomol. NMR* **28,** 341–355
25. Stuart, A. C., Borzilleri, K. A., Withka, J. M., and Palmer, A. G., 3rd (1999) Compensating for variations in $^{1}H$-$^{13}C$ scalar coupling constants in isotope-filtered NMR experiments. *J. Am. Chem. Soc.* **121,** 5346–5347
26. Güntert, P., Mumenthaler, C., and Wüthrich, K. (1997) Torsion angle dynamics for NMR structure calculation with the new program DYANA. *J. Mol. Biol.* **273,** 283–298
27. Herrmann, T., Güntert, P., and Wüthrich, K. (2002) Protein NMR structure determination with automated NOE assignment using the new software CANDID and the torsion angle dynamics algorithm DYANA. *J. Mol. Biol.* **319,** 209–227
28. Güntert, P. (2009) Automated structure determination from NMR spectra. *Eur. Biophys. J.* **38,** 129–143
29. Brünger, A. T., Adams, P. D., Clore, G. M., DeLano, W. L., Gros, P., Grosse-Kunstleve, R. W., Jiang, J. S., Kuszewski, J., Nilges, M., Pannu, N. S., Read, R. J., Rice, L. M., Simonson, T., and Warren, G. L. (1998) Crystallography & NMR system: a new software suite for macromolecular structure determination. *Acta Crystallogr. D* **54,** 905–921
30. Lüthy, R., Bowie, J. U., and Eisenberg, D. (1992) Assessment of protein models with three-dimensional profiles. *Nature* **356,** 83–85
31. Sippl, M. J. (1993) Recognition of errors in three-dimensional structures of proteins. *Proteins* **17,** 355–362
32. Laskowski, R. A., MacArthur, M. W., Moss, D. S., and Thornton, J. M. (1993) *PROCHECK*: a program to check the stereochemical quality of protein structures. *J. Appl. Crystallogr.* **26,** 283–291
33. Lovell, S. C., Davis, I. W., Arendall, W. B., 3rd, de Bakker, P. I., Word, J. M., Prisant, M. G., Richardson, J. S., and Richardson, D. C. (2003) Structure validation by Cα geometry: φ, ψ, and Cβ deviation. *Proteins* **50,** 437–450
34. Bhattacharya, A., Tejero, R., and Montelione, G. T. (2007) Evaluating protein structures determined by structural genomics consortia. *Proteins* **66,** 778–795
35. Huang, Y. J., Powers, R., and Montelione, G. T. (2005) *J. Am. Chem. Soc.* **127,** 1665–1674
36. Englander, S. W., Sosnick, T. R., Englander, J. J., and Mayne, L. (1996) Mechanisms and uses of hydrogen exchange. *Curr. Opin. Struct. Biol.* **6,** 18–23
37. Pantazatos, D., Kim, J. S., Klock, H. E., Stevens, R. C., Wilson, I. A., Lesley, S. A., and Woods, V. L., Jr. (2004) Rapid refinement of crystallographic protein construct definition employing enhanced hydrogen/deuterium exchange MS. *Proc. Natl. Acad. Sci. U.S.A.* **101,** 751–756
38. Spraggon, G., Pantazatos, D., Klock, H. E., Wilson, I. A., Woods, V. L., Jr., and Lesley, S. A. (2004) On the use of DXMS to produce more crystallizable proteins: structures of the *T. maritima* proteins TM0160 and TM1171. *Protein Sci.* **13,** 3187–3199
39. Valafar, H., and Prestegard, J. H. (2004) REDCAT: a residual dipolar coupling analysis tool. *J. Magn. Reson* **167,** 228–241
40. Kornhaber, G. J., Snyder, D., Moseley, H. N., and Montelione, G. T. (2006) Identification of zinc-ligated cysteine residues based on $^{13}C\alpha$ and $^{13}C\beta$ chemical shift data. *J. Biomol. NMR* **34,** 259–269
41. Sharma, D., and Rajarathnam, K. (2000) $^{13}C$ NMR chemical shifts can predict disulfide bond formation. *J. Biomol. NMR* **18,** 165–171
42. Israël, A. (2010) The IKK complex, a central regulator of NF-κB activation. *Cold Spring Harb. Perspect. Biol.* **2,** a000158
43. Hiscott, J. (2007) Convergence of the NF-κB and IRF pathways in the regulation of the innate antiviral response. *Cytokine Growth Factor Rev.* **18,** 483–490
44. Sharma, S., tenOever, B. R., Grandvaux, N., Zhou, G. P., Lin, R., and Hiscott, J. (2003) Triggering the interferon antiviral response through an IKK-related pathway. *Science* **300,** 1148–1151
45. Eddy, S. F., Guo, S., Demicco, E. G., Romieu-Mourez, R., Landesman-Bollag, E., Seldin, D. C., and Sonenshein, G. E. (2005) Inducible IκB kinase/IκB kinase ε expression is induced by CK2 and promotes aberrant nuclear factor-κB activation in breast cancer cells. *Cancer Res.* **65,** 11375–11383
46. Adli, M., and Baldwin, A. S. (2006) IKK-i/IKKε controls constitutive, cancer cell-associated NF-κB activity via regulation of Ser-536 p65/RelA phosphorylation. *J. Biol. Chem.* **281,** 26976–26984
47. Boehm, J. S., Zhao, J. J., Yao, J., Kim, S. Y., Firestein, R., Dunn, I. F., Sjostrom, S. K., Garraway, L. A., Weremowicz, S., Richardson, A. L., Greulich, H., Stewart, C. J., Mulvey, L. A., Shen, R. R., Ambrogio, L., Hirozane-Kishikawa, T., Hill, D. E., Vidal, M., Meyerson, M., Grenier, J. K., Hinkle, G., Root, D. E., Roberts, T. M., Lander, E. S., Polyak, K., and Hahn, W. C. (2007) Integrative genomic approaches identify *IKBKE* as a breast cancer oncogene. *Cell* **129,** 1065–1079
48. Gasteiger, E., Gattiker, A., Hoogland, C., Ivanyi, I., Appel, R. D., and Bai-

roch, A. (2003) ExPASy: the proteomics server for in-depth protein knowledge and analysis. *Nucleic Acids Res.* **31,** 3784–3788
49. Olsen, J. V., Vermeulen, M., Santamaria, A., Kumar, C., Miller, M. L., Jensen, L. J., Gnad, F., Cox, J., Jensen, T. S., Nigg, E. A., Brunak, S., and Mann, M. (2010) Quantitative phosphoproteomics reveals widespread full phosphorylation site occupancy during mitosis. *Sci. Signal.* **3,** ra3
50. Dunker, A. K., Brown, C. J., Lawson, J. D., Iakoucheva, L. M., and Obradović, Z. (2002) Intrinsic disorder and protein function. *Biochemistry* **41,** 6573–6582
51. Xie, H., Vucetic, S., Iakoucheva, L. M., Oldfield, C. J., Dunker, A. K., Uversky, V. N., and Obradovic, Z. (2007) Functional anthology of intrinsic disorder. 1. Biological processes and functions of proteins with long disordered regions. *J. Proteome Res.* **6,** 1882–1898
52. Dunker, A. K., and Obradovic, Z. (2001) The protein trinity-linking function and disorder. *Nat. Biotechnol.* **19,** 805–806
53. Ezeokonkwo, C., Zhelkovsky, A., Lee, R., Bohm, A., and Moore, C. L. (2011) A flexible linker region in Fip1 is needed for efficient mRNA polyadenylation. *RNA* **17,** 652–664
54. Zhou, H. X. (2001) The affinity-enhancing roles of flexible linkers in two-domain DNA-binding proteins. *Biochemistry* **40,** 15069–15073
55. Gokhale, R. S., and Khosla, C. (2000) Role of linkers in communication between protein modules. *Curr. Opin. Chem. Biol.* **4,** 22–27
56. Fong, J. H., and Panchenko, A. R. (2010) Intrinsic disorder and protein multibinding in domain, terminal, and linker regions. *Mol. BioSyst.* **6,** 1821–1828
57. Dunker, A. K., Cortese, M. S., Romero, P., Iakoucheva, L. M., and Uversky, V. N. (2005) The roles of intrinsic disorder in protein interaction networks. *FEBS J.* **272,** 5129–5148
58. Kriwacki, R. W., Hengst, L., Tennant, L., Reed, S. I., and Wright, P. E. (1996) Structural studies of $p21^{Waf1/Cip1/Sdi1}$ in the free and Cdk2-bound state: conformational disorder mediates binding diversity. *Proc. Natl. Acad. Sci. U.S.A.* **93,** 11504–11509
59. Lacy, E. R., Filippov, I., Lewis, W. S., Otieno, S., Xiao, L., Weiss, S., Hengst, L., and Kriwacki, R. W. (2004) p27 binds cyclin-CDK complexes through a sequential mechanism involving binding-induced protein folding. *Nat. Struct. Mol. Biol.* **11,** 358–364
60. Galea, C. A., Wang, Y., Sivakolundu, S. G., and Kriwacki, R. W. (2008) Regulation of cell division by intrinsically unstructured proteins: intrinsic flexibility, modularity, and signaling conduits. *Biochemistry* **47,** 7598–7609
61. Wang, Y., Fisher, J. C., Mathew, R., Ou, L., Otieno, S., Sublet, J., Xiao, L., Chen, J., Roussel, M. F., and Kriwacki, R. W. (2011) Intrinsic disorder mediates the diverse regulatory functions of the CDK inhibitor p21. *Nat. Chem. Biol.* **7,** 214–221
62. Huang, Y. J., Hang, D., Lu, L. J., Tong, L., Gerstein, M. B., and Montelione, G. T. (2008) Targeting the human cancer pathway protein interaction network by structural genomics. *Mol. Cell. Proteomics* **7,** 2048–2060
63. Zweckstetter, M., and Bax, A. (2000) Prediction of sterically induced alignment in a dilute liquid crystalline phase: aid to protein structure determination by NMR. *J. Am. Chem. Soc.* **122,** 3791–3792